

Experimental support for a simplified approach to CTRW transport models and exploration of parameter interpretation

Scott K. Hansen¹

¹Ben-Gurion University of the Negev

November 21, 2022

Abstract

We empirically test our earlier theoretical arguments about simplification of continuous-time random walk (CTRW) solute transport models, namely that without loss of generality the velocity-like term may be set to mean groundwater velocity, the dispersion-like term defined by a classical, velocity-independent dispersivity, and the so-called time constant, τ , set to unity. We also argue that for small-scale heterogeneous advection (HA) and mobile-immobile mass transfer (MIMT) CTRW transition time distributions, $\Psi(t)$, are unaffected by mean flow velocity. To experimentally test these claims, we re-analyze two bench-scale transport experiments—one for HA, one for MIMT—each performed at multiple flow rates in otherwise identical conditions, and show it is possible to simultaneously explain all breakthrough curves in each, subject to the above constraints. We compare our calibrations with earlier efforts for the same data sets. In the HA calibration we identify a $\Psi(t)$ of the same functional form as previous authors, and which yielded breakthrough predictions essentially identical to theirs, but with greatly differing parameters. This illustrates how values of individual CTRW parameters may not map one-to-one onto underlying physics. We recommend reporting complete model descriptions, discuss how the simplified approach assists in this and other theoretical considerations.

Abstract

We empirically test our earlier theoretical arguments about simplification of continuous-time random walk (CTRW) solute transport models, namely that without loss of generality the velocity-like term, v_ψ , may be set to mean groundwater velocity, the dispersion-like term, D_ψ , defined by a classical, velocity-independent dispersivity, and the so-called time constant, τ , to unity. We also argue that for small-scale heterogeneous advection (HA) and mobile-immobile mass transfer (MIMT) CTRW transition time distributions, $\psi(t)$, are unaffected by mean flow velocity. To experimentally test these claims, we re-analyze two bench-scale transport experiments—one for HA, one for MIMT—each performed at multiple flow rates in otherwise identical conditions, and show it is possible to simultaneously explain all breakthrough curves in each, subject to the above constraints. We compare our calibrations with earlier efforts for the same data sets. In the HA calibration we identify a $\psi(t)$ of the same functional form as previous authors, and which yielded breakthrough predictions essentially identical to theirs, but with greatly differing parameters. This illustrates how values of individual CTRW parameters may not map one-to-one onto underlying physics. We recommend reporting complete model descriptions, discuss how the simplified approach assists in this and other theoretical considerations.

1 Introduction

In a recent paper (Hansen, 2020), we proposed an interpretation of some of the terms of the continuous-time random walk (CTRW) generalized master equation (GME), which allow its 1D form to be written in the following simplified way:

$$\frac{\partial c(x, t)}{\partial t} = \int_0^t M(t - t') \left(-\bar{v} \frac{\partial c(x, t')}{\partial x} + \alpha \bar{v} \frac{\partial^2 c(x, t')}{\partial x^2} \right) dt'. \quad (1)$$

Here, c [ML^{-3}] is concentration, $M(t)$ [T^{-1}] is a temporal memory function, \bar{v} [LT^{-1}] is mean groundwater velocity, and α [L] is a standard Fickian dispersivity, generated by multiplication of \bar{v} by some fixed, medium-specific dispersivity, α [L]; x [L] is spatial coordinate, and t [T] is time. On this approach, $M(t)$ is defined in the Laplace domain according to the formula:

$$\tilde{M}(s) \equiv \frac{s\tilde{\psi}(s)}{1 - \tilde{\psi}(s)}, \quad (2)$$

where superscript tilde denotes the Laplace transform, s [T^{-1}] is the Laplace variable, and $\psi(t)$ [T^{-1}] is the probability distribution function for a subordination mapping representing

41 the total time taken for solute to complete a transition that would have taken unit time
 42 under purely advective-dispersive physics as described by \bar{v} and α .

43 This approach simplifies and physically constrains the CTRW GME in a number
 44 of ways and also provides an interpretation to its parameters. By contrast, in typical usage:
 45 (a) the \bar{v} and $\alpha\bar{v}$ are replaced with arbitrary fitting parameters v_ψ and D_ψ that do not
 46 generally have any specific relation to groundwater velocity, (b) the definition of M typically
 47 contains an arbitrary “time constant” fitting parameter with no specific interpretation,
 48 τ [T], in its numerator, and (c) the transition time distribution, $\psi(t)$ has no particular
 49 definition; it is an additional fitting “parameter”. For clarity, the standard CTRW GME
 50 and transformed memory function corresponding to (1-2) are

$$\frac{\partial c(x, t)}{\partial t} = \int_0^t M(t - t') \left(v_\psi \frac{\partial c(x, t')}{\partial x} + D_\psi \frac{\partial^2 c(x, t')}{\partial x^2} \right) dt', \quad (3)$$

51

$$\tilde{M}(s) \equiv \frac{s\tau\tilde{\psi}(s)}{1 - \tilde{\psi}(s)}. \quad (4)$$

52 Implicitly τ is set to unity in the simplified approach, so the units remain consistent. The
 53 simplified approach is based on two ideas which are outlined in more detail in Hansen
 54 (2020):

- 55 1. It is possible to select the time constant τ so that v_ψ and D_ψ are equal to their
 56 Fickian counterparts.
- 57 2. The memory function (4) is invariant under the simultaneous transformations $\tau \rightarrow$
 58 $1, \tilde{\psi}(s) \rightarrow [\tilde{\psi}(s)]^{1/\tau}$.

59 Two key subsurface transport processes that need to be captured by $\psi(t)$ are (the
 60 non-Fickian portion of) local-scale heterogeneous advection (HA), and mobile-immobile
 61 mass transfer (MIMT). Elsewhere (Hansen and Berkowitz, 2020b,0), in describing the
 62 CTRW-on-a-streamline approach, have argued that both advective heterogeneity and
 63 MIMT (including behavior described by multi-rate mass transfer, first-order non-equilibrium
 64 mass transfer, and retardation) can be adequately captured by a subordination approach.

65 We do not believe it has been remarked upon, but a joint implication of the subordination
 66 mapping interpretation of $\psi(t)$ alongside the CTRW-on-a-streamline arguments is that
 67 $\psi(t)$ should be invariant to mean groundwater velocity under many scenarios. For MIMT,
 68 so long as immobilization probability is related to time-in-system rather than distance
 69 traveled and the immobilization time pdf is determined by conditions in the immobile

70 domain alone, it follows that the distribution of delay times due to the MIMT physics
 71 is independent of the mean flow velocity in the mobile domain. For HA, it follows from
 72 linearity of the groundwater flow equation that velocity fluctuations will scale with fluctuations
 73 in the local mean groundwater velocity. We may arbitrarily define a transition to have
 74 occurred when solute has traveled $d(\bar{v})$ [L] units along its streamline, where $d(\bar{v})$ is selected
 75 as the distance that advection covers in unit time at mean velocity. Because all the velocities
 76 scale with \bar{v} , $\psi(t)$, defined as the probability distribution for the actual time taken to complete
 77 a transition of length d , is unchanged with changes in \bar{v} .

78 The argument above generates testable predictions. If tracer experiments are to
 79 be performed across a tank or column under multiple flow rates but otherwise identical
 80 conditions, we would expect all the breakthrough curves obtained at the various flow rates
 81 to be explained by a single $\psi(t)$, α , and the actual \bar{v} values from the various experiments.
 82 Consequently, in this paper we re-analyze results from two experiments that were conducted
 83 repeatedly at multiple flow rates: one featuring HA in sand, and one featuring MIMT
 84 in the form of matrix diffusion.

85 For HA, few existing bench-scale data sets were available. A few experiments considered
 86 breakthrough at multiple distances in the same apparatus (Silliman and Simpson, 1987;
 87 Huang *et al.*, 1995). However, to our knowledge, Levy and Berkowitz (2003) present the
 88 only data on breakthrough curves obtained at multiple flow rates in the same statistically
 89 stationary, heterogeneous flow cell. We used this experimental data set for our analyses.
 90 For MIMT, a greater variety of published data was available. Both van Genuchten *et al.*
 91 (1977) and Gaber *et al.* (1995) present data for non-equilibrium mass transfer experiments
 92 performed at multiple flow rates in the same apparatus. These results were analyzed in
 93 the CTRW context by Li and Ren (2009), though the calibrations presented featured wide
 94 variation in CTRW parameters between runs at different flow rates and between, e.g.,
 95 \bar{v} and v_ψ . While it would be worthwhile to re-analyze this data, we obtained data from
 96 the more recent column experiments of Knorr *et al.* (2016), which had never been analyzed
 97 in the context of CTRW, and which featured a complex dual-domain geometry that appeared
 98 to represent a more difficult fitting challenge. We chose to calibrate against this data set
 99 for the MIMT demonstration.

100 We corroborate the simplified approach and our claims about velocity invariance
 101 of $\psi(t)$ by successfully calibrating all the breakthrough curves simultaneously with identical

102 parameters for both data sets. We also calibrate very different CTRW parameters than
 103 presented by Berkowitz and Scher (2009) for the same system, illustrating that it is not
 104 generally possible to interpret particular parameters in terms of system features, independent
 105 of a complete model description. Rather, in line with the temporal subordination philosophy
 106 underlying the simplified approach, the complete CTRW GME parameterization must
 107 be viewed as a whole.

108 2 Heterogeneous advection flow cell experiment

109 2.1 Experimental setup

110 The data set was obtained from a suite of experiments previously discussed at length
 111 by Levy and Berkowitz (2003). We will only briefly recapitulate the relevant factors in
 112 the experimental setup, as full details may be found in the original paper. Tracer experiments
 113 were performed in a flow cell with length $L = 2.13$ m, which was manually packed with
 114 “blocks”, each of which consisted of one of three different sands with different hydraulic
 115 conductivities. The blocks were arranged in the flow cell in such a way that a heterogeneous
 116 but spatially stationary conductivity field with an exponential correlation structure was
 117 created. Levy and Berkowitz reported flow rates for the three experiments in this cell
 118 as 175 ml min^{-1} , 74 ml min^{-1} , and 11 ml min^{-1} . Bulk cross-sectional area of the flow cell
 119 was reported as 650 cm^2 , allowing Darcy flux q to be computed. Actual system porosity,
 120 n , was not measured or estimated, so actual average fluid velocity, \bar{v} , is not exactly known.

121 2.2 Numerical approach

122 Our goal was to numerically re-analyze these experimental results and explain all
 123 the breakthrough curves simultaneously under tight constraints: *identical* $\psi(t)$ and α ,
 124 and exactly enforcing $v_\psi = \bar{v} = q/n$, for some fixed n , and $D_\psi \equiv D = \alpha\bar{v}$.

125 Fitting was performed by numerical Laplace transform inversion. The analytic solution
 126 of the GME (1) in the Laplace domain for a 1D semi-infinite domain has the form (Burnell
 127 *et al.*, 2017):

$$\tilde{c}(x, s) = \frac{1}{s} \exp \left\{ \frac{x}{2D} \left[\bar{v} - \sqrt{\bar{v}^2 + \frac{4Ds}{\tilde{M}(s)}} \right] \right\} \quad (5)$$

128 where $\tilde{M}(s)$ is as defined in (2). Based on past success, we assumed that $\psi(t)$ had truncated
 129 power law (TPL) form. The Laplace transform of the TPL is (Dentz *et al.*, 2004):

$$\tilde{\psi}(s) = (1 + t_2 s)^\beta \exp(t_1 s) \frac{\Gamma(-\beta, t_1 s + t_1 t_2^{-1})}{\Gamma(-\beta, t_1 t_2^{-1})}. \quad (6)$$

130 Note that whilst we assume that τ is unity, we do not assume that this is equal to the
 131 t_1 parameter of the TPL, in contrast with some earlier literature. In our approach, $\psi(t)$
 132 is understood as a temporal subordination mapping corresponding to unit time, and all
 133 its parameters may be freely specified.

134 For a given vector of parameters, we determined the estimate $\hat{c}(x = L, t; \alpha, \beta, t_1, t_2, \bar{v})$
 135 by numerical inversion of the Laplace transform (5) using the Fixed Talbot algorithm
 136 (Abate and Valkó, 2004) at the locations where breakthrough concentration measurements
 137 had been made. To optimize the fitting parameters, α , β , t_1 , t_2 , and n , we defined an
 138 equally-weighted penalty function based on the squared distance of all measured breakthrough
 139 curve data from $\hat{c}(x = L, t_i; \alpha, \beta, t_2, \bar{v})$, where t_i represents the i -th measurement time
 140 in the corresponding breakthrough curve. We used the Nelder-Mead unconstrained optimization
 141 algorithm (Nelder and Mead, 1965), as implemented in Numpy/Scipy (Oliphant, 2007),
 142 to iteratively update the five fitting parameters to improve the model fit relative to the
 143 data. The fitting parameters were represented internally as squares of dummy variables
 144 to enforce non-negativity.

145 2.3 Results and discussion

146 The optimization algorithm found a best fit with the parameters $\alpha = 5.587 \times 10^{-2}$
 147 m, $t_1 = 1.154$ min, $t_2 = 4.011$ min, and $\beta = 0.556$, inferring porosity $n = 0.245$. In
 148 Figure 1, the experimental data are shown, along with the best fit $\hat{c}(L, t)$. It is apparent
 149 from the figure that the fitted \hat{c} yields a qualitatively good fit across the all breakthrough
 150 curves. Note that despite the TPL form, the modest t_2 (representing the onset time of
 151 exponential tempering) means that this distribution is close to exponential. This accounts
 152 for the relative similarity of the empirical breakthrough curves ADE breakthrough curves,
 153 as demonstrated by Levy and Berkowitz, and expected for advection through ten or more
 154 correlation lengths of moderately heterogeneous media (see Hansen *et al.*, 2018, and references
 155 within). When $\psi(t) = e^{-t}$, it follows from (2) that $\tilde{M}(s) = 1$, or $M(t) = \delta(t)$, and
 156 the CTRW GME reduces to the ADE.

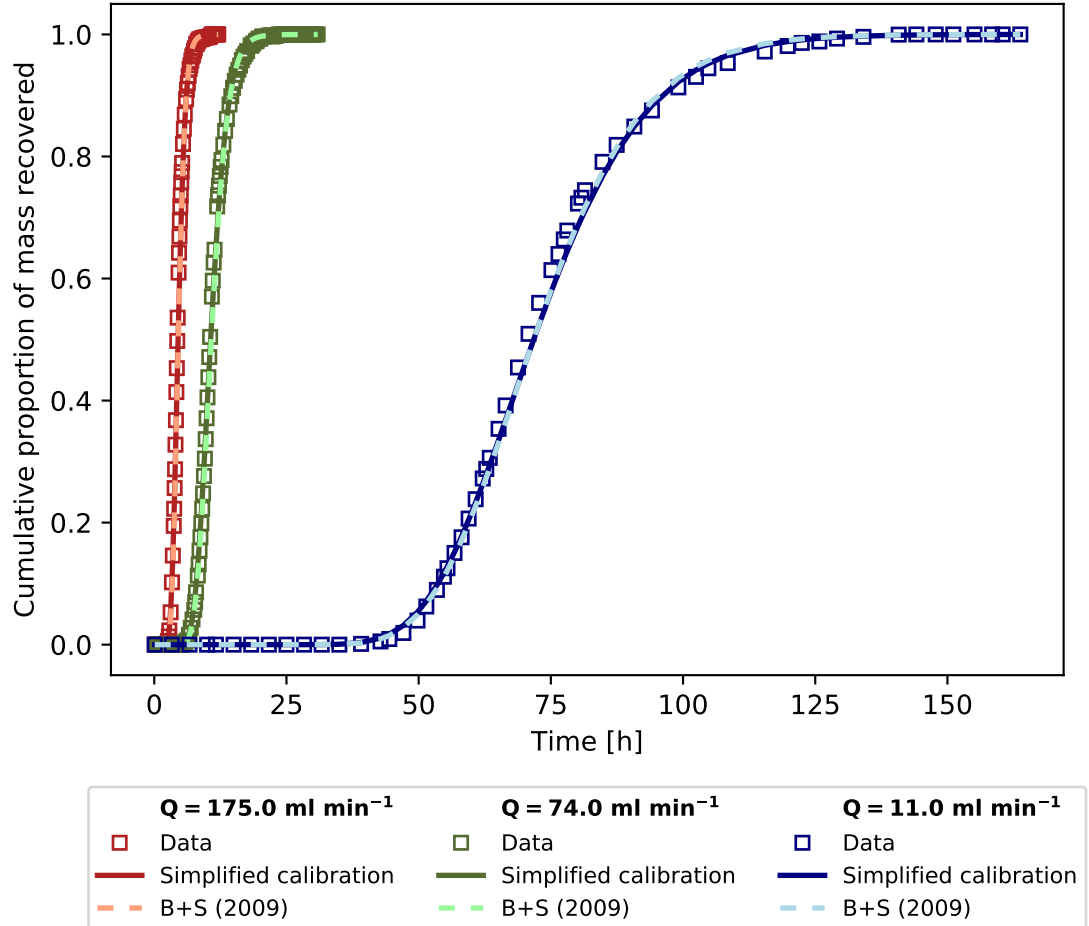


Figure 1. Simultaneous fit of three breakthrough curves collected in the flow cell described by Levy and Berkowitz (2003), at three different flow rates. Empirical breakthrough data points are indicated by hollow squares, and corresponding predicted breakthrough curves are shown as solid lines; both are colour-coded according to the corresponding flow rate. All three fitted curves shared identical $\alpha = 5.587 \times 10^{-2} \text{ m}$, fitted porosity $n = 0.245$, and TPL-distributed $\psi(t)$ (6) with parameters $t_1 = 1.154 \text{ min}$, $t_2 = 4.011 \text{ min}$, $\beta = 0.556$.

157 Berkowitz and Scher (2009) previously analyzed the same data and were able to
 158 obtain excellent fits to the breakthrough curves with separate TPL $\psi(t)$ for each flow
 159 rate that nevertheless shared two of their three parameters (t_1 was allowed to vary). We
 160 recomputed the v_ψ values reported in the original paper to three significant digits, enforcing
 161 $v_\psi \propto Q$ and $D_\psi \propto v_\psi$, each with single constants of proportionality for all three flow
 162 rates (a stipulation mentioned explicitly by the authors) by adjusting the constants of
 163 proportionality so as to generate excellent fits that closely match the published fits. We
 164 use these recomputed v_ψ values alongside the other exact, published numbers in all analyses.

165 The Berkowitz and Scher approach differs from ours in two major ways:

- 166 1. The earlier paper considered a “transition” to correspond to a fixed, pore-sized
 167 motion, with τ representing a characteristic time for such a motion (which naturally
 168 varies inversely with velocity). The t_1 parameter in defining the TPL $\psi(t)$ was also
 169 understood to be identified with this quantity, so $t_1 = \tau$, and varied with velocity
 170 also. By contrast, on what we dub the simplified approach, τ is understood as unit
 171 *time*, the “transition” representing notional motion occurring in unit time under
 172 macroscopic advective-dispersive conditions, and $\psi(t)$ as a mapping to the actual
 173 time taken to complete that motion with all physics operative. this temporal mapping
 174 perspective supports the velocity-invariance of $\psi(t)$, as well as the independence
 175 of all its parameters from τ (which could be set arbitrarily, but is always set to
 176 unity for convenience).
- 177 2. We take v_ψ as *identified* with an actual groundwater flow velocity, and α as a fixed,
 178 velocity independent scattering rate that is a medium property. This was explicitly
 179 not the conception of Berkowitz and Scher, who estimated a systematically different
 180 mean flow velocity based on an alternative measure of porosity. That said, actual
 181 mean flow velocity cannot be directly measured, only estimated from a given flow
 182 rate and porosity. and the v_ψ used by Berkowitz and Scher could also be interpreted
 183 as a true flow velocity by use of a plausible value of porosity.

184 It is enlightening to compare our fits with the strikingly different ones presented
 185 by Berkowitz and Scher; see Table 1 for a comparison of fitted parameters. Notably, the
 186 distinct TPL $\psi(t)$ functions obtained for each value of Q obtained by Berkowitz and Scher
 187 for pore-scale transitions feature a lengthy power law regime and a power law exponent

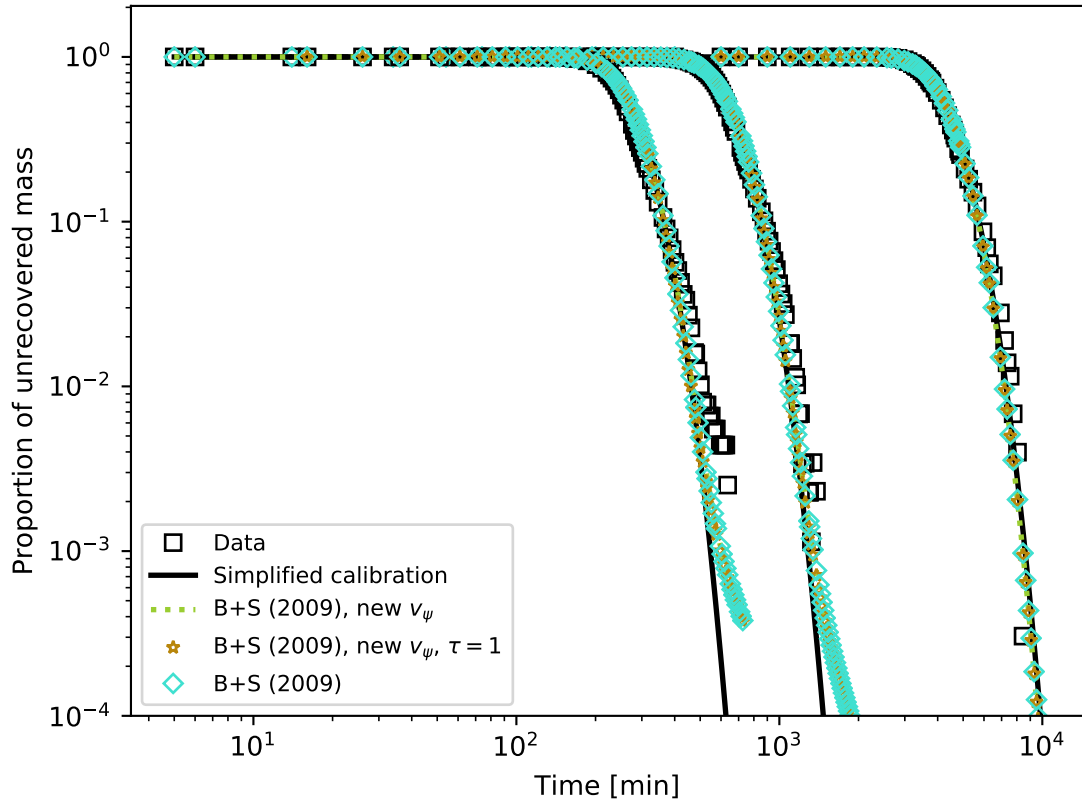


Figure 2. Comparison of ensembles of fitted breakthrough curves for all three flow rates, shown using different parameterization approaches. Curves are shown as complementary CDFs on log-log axes to highlight the tail regions. The three column groups in Table 1 are each represented, as well as a fourth approach that rescales the Berkowitz and Scher results to correspond with the velocity in the simplified calibration *and* $\tau = 1$.

188 $\beta = 1.6$, whereas our unified TPL fit features a much smaller value $\beta = 0.556$ and a
 189 negligible power law regime.

190 The breakthrough curves obtained with the velocity-dependent parameterizations
 191 of Berkowitz and Scher are visually indistinguishable from curves obtained with the simplified
 192 approach shown in Figure 1. The theoretical non-uniqueness of CTRW parameterization
 193 has previously been remarked upon (Hansen and Berkowitz, 2014). However, to our knowledge
 194 this is the first instance of near-identical calibrations being produced with completely
 195 distinct $\psi(t)$ functions. It may be initially surprising that the earlier calibrations featured

lengthy power law regions in their $\psi(t)$, whereas the new calibration does not. However, we note that because we make the identification $\tau = 1$, the implied distance covered during a transition is much larger (on the order of 10 cm at the fastest flow rate), compared with that of Berkowitz and Scher, who anticipated transitions on the order of a single pore. Consequently, much self-averaging of pore-scale transitions occur over a single notional transition on the simplified approach with $\tau = 1$. Prior to the self-averaging, CTRW parameters such as β remain meaningful as to the distribution of transition times across their implicit support scale.

In Figure 2 we compare the tail behavior of (i) our simplified approach parameterization, (ii) the parameterizations presented by Berkowitz and Scher, (iii) those same parameterizations modified to use the same v_ψ 's as we did, (iv) further modified to correspond to unit τ . The latter three are identical, as the theory in Hansen (2020) predicts, and all four are essentially the same even within the tail region of the measurements. We also compare the $\psi(t)$ distributions for (i), (iii) and (iv) in Figure 3. Strikingly, we see all the distributions in (ii) map onto one-another under the transformations (iv), which follows from their being physically meaningful for their various flow rates and now sharing the same v_ψ , α , and τ . However, the $\psi(t)$ distribution predicted by (i) remains totally distinct, despite only varying in its underlying α from the transformed distributions (iv).

An important take-away from this analysis is that efforts to directly connect single parameters such as β to fundamental transport characteristics are too simple: it is crucial to consider the complete mapping $\tau \rightarrow \psi(t)$ and also the underlying ADE model. As we have seen, even small changes in the chosen α with otherwise identical v_ψ and τ cause drastic quantitative and qualitative changes to the $\psi(t)$ distribution needed to accurately describe observed physics.

3 Mobile-immobile column experiment

3.1 Experimental setup

Source data was obtained for a set of MIMT column experiments detailed in Knorr *et al.*; we refer readers to the original paper for more details regarding experimental setup. In brief, tracer experiments were performed in a cylindrical column whose core (mobile domain) was filled with large class beads, surrounded by an annular immobile region packed with clayey silt. The core had a radius of 1.6 cm, and the outer annulus filled the region whose radial distance from the axis was between 1.6 and 4.4 cm from the axis of the column,

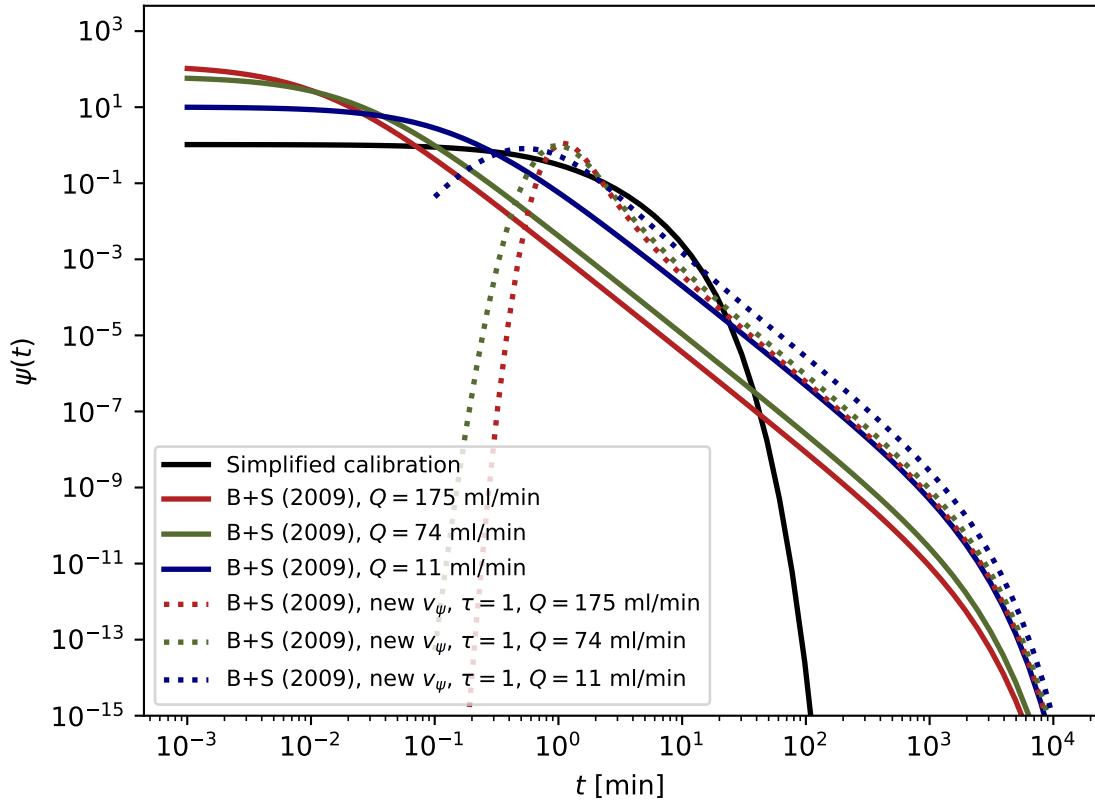


Figure 3. Comparison of transition functions, $\psi(t)$. Solid lines represent curves defined in the *Simplified calibration* (all share the same $\psi(t)$) and *B+S (2009)* column groups in Table 1. Dotted curves represent the $\psi(t)$ of B+S, interpreted according to the simplified approach; modified to share the same velocities as the simplified calibration, and also transformed in Laplace space to share the same unit value of τ .

Table 1. Comparison of fitted parameters explaining the breakthrough curves in the flow cell, as presented in this work (*Simplified calibration* meta-column), in Berkowitz and Scher, except with corrected v_ψ (*B+S (2009)* meta-column), and Berkowitz and Scher, rescaled to match the v_ψ employed in the simplified calibration (*B+S (2009)*, *S.C. v ψ* meta-column).

Q [ml min ⁻¹]	Simplified calibration			B+S (2009), $v_\psi = \text{S.C. } \bar{v}$			B+S (2009) ¹		
	11	74	175	11	74	175	11	74	175
\bar{v}^2 [m min ⁻¹]	6.91e-4	4.65e-3	1.10e-2	6.91e-4	4.65e-3	1.10e-2	7.91e-4	5.31e-3	1.26e-2
n [-]		0.245			0.245			0.214	
α [m]		5.59e-2			5.05e-2			5.05e-2 ³	
τ [min]		1		1.81e-2	2.87e-2	1.44e-2	1.58e-1	2.51e-2	1.26e-2
t_1 [min]		1.155		1.58e-1	2.51e-2	1.26e-2	1.58e-1	2.51e-2	1.26e-2
t_2 [min]		4.011			1000			1000	
β [-]		0.556			1.6			1.6	

¹ Corrected velocities shown. ² Equivalently, v_ψ . ³ From interpreting v_ψ as actual mean flow velocity, \bar{v} .

228 where it abutted a layer of silicon glue that attached it to the inner wall of the impermeable
 229 column. The column itself had internal length, L of 50 cm, with tracer-enriched fluid pumped
 230 at constant rates into the mobile domain at one end of the column and collected at the
 231 other. By measuring tracer concentrations at the column exit, breakthrough curves were
 232 obtained for a number of chemical species, each tested at volumetric flow rates of 104.4,
 233 21, and 7.2 ml h⁻¹. The authors estimated the porosity, n , of the mobile domain as approximately
 234 $n = 0.44 \pm 1$ based on geometrical considerations and water displacement measurements.

235 We noted that the raw breakthrough data published by Knorr *et al.*, exhibited an
 236 implied arrival-time PDF whose integral over the real line was less than one for some flow
 237 rates, which affected the cumulative recovery time series we employed for calibration.
 238 We discuss how we rescaled the data in Appendix A. All analysis was performed using
 239 the rescaled data.

240 The models assumed a well-mixed mobile zone that can be treated as a 1D feature.
 241 Based on the calibrated dispersivities presented by the authors of the experimental study,
 242 we calculated that molecular diffusion was necessary to augment transverse dispersion
 243 in mixing the mobile zone of the column. Consequently, we selected the experimental

244 time series employing a deuterium tracer, as this species featured the largest Fickian diffusivity
 245 of those studied.

246 3.2 Numerical approach

247 Analysis was again performed by making use of the 1D analytic solution (5) for the
 248 breakthrough curve at the outlet of the column. We employed the assumption that the
 249 distribution of time between immobilization events (or until first immobilization) was
 250 exponentially distributed with parameter λ . In Appendix B we derive the Laplace transform
 251 of the sojourn time pdf for a single immobilization event as:

$$\tilde{\phi}(s) \equiv 1 - \frac{\sqrt{2\mu s}}{s + \mu}, \quad (7)$$

252 with μ [T^{-1}] is a free parameter proportional to the Fickian diffusion constant in the immobile
 253 zone. The CTRW transition time distribution was defined according to the relation (Margolin
 254 *et al.*, 2003; Boano *et al.*, 2007)

$$\tilde{\psi}(s) = \tilde{\psi}_0(s + \lambda - \lambda\tilde{\phi}(s)), \quad (8)$$

255 where $\psi_0(t)$ is the transition time distribution in the absence of MIMT. In our case, MIMT
 256 is assumed to be the only non-Fickian process, so

$$\tilde{\psi}_0(s) = \frac{1}{1 + s}. \quad (9)$$

257 as this choice causes (2) to become unity, and (1) to thus degenerate into the ADE.

258 We used a similar numerical approach and algorithm to that detailed above for the
 259 flow cell experiment, with a duly modified $\tilde{\psi}(s)$. In accordance with Knorr *et al.*, we manually
 260 set $n = 0.43$ and performed Nelder-Mead automated fitting of all empirical breakthrough
 261 curves simultaneously, using the published flow rates for each experiment, to identify α ,
 262 λ , and d shared by all experiments.

263 For comparison, we evaluated the analytical solution of Maloszewski and Zuber (1990),
 264 which was used by Knorr *et al.* to explain their experimental data. Their solution for
 265 the CDF corresponding to the CTRW model (5) may be expressed as

$$\hat{c}_{MZ}(x, t) = \frac{a}{2\pi} \sqrt{\frac{x^2}{\alpha\bar{v}}} \int_0^t \int_0^s \exp \left[-\frac{(x - u\bar{v})}{4\alpha u\bar{v}} - \frac{a^2 u^2}{s - u} \right] \frac{1}{u(s - u)^3} du ds, \quad (10)$$

Table 2. Comparison of fitted parameters for the ensemble of curves from the MIMT column experiment. The parameters identified in this work are listed in the *Simplified calibration* meta-column, and those identified by Knorr *et al.* (2016) are listed in the corresponding meta-column. Fitted parameters from that paper have been refactored in terms of n and α for easier comparison. Note that the reported n values are explicitly identified as effective mobile porosities in Knorr *et al.*.

		Simplified calibration			Knorr <i>et al.</i> (2016)		
		7.2	21	104.4	7.2	21	104.4
Q	[cm ³ h ⁻¹]						
v_ψ	[cm h ⁻¹]	2.08	6.08	30.2	2.38	6.24	29.17
n	[—]		0.43		0.376	0.418	0.445
α	[cm]		1.30		7.6e-2	0.106	0.303
λ	[h ⁻¹]		4.11			-	
μ	[h ⁻¹]		1.03e3			-	
a	[h ^{-1/2}]			-	0.105	0.100	9.48e-2

266 where a [T^{-1/2}] is a free parameter that scales with the square root of the dispersivity
 267 in the matrix. As this solution is defined in terms of a double-integral with an integrand
 268 that varies over many orders of magnitude, we employed the `mpmath` arbitrary-precision
 269 Python library (Johansson *et al.*, 2021) to perform the numerical quadrature.

270 3.3 Results and discussion

271 The optimized parameters are listed in Table 2, alongside the parameters determined
 272 by Knorr *et al.*. Predicted breakthrough curves for the ensemble of flow rates as compared
 273 with the (corrected) data is seen in Figure 4. The comparable fidelity of the two sets of
 274 curves is apparent, despite the fact that the earlier authors allowed substantial variation
 275 in what should be flow-rate-independent parameters to optimize their fits, and we did
 276 not. We observe that our model contains one more degree of freedom than the Maloszewski
 277 and Zuber model, in that it contains a distinct capture rate parameter. This is opposed
 278 to assuming the mobile domain is well-mixed, with net fluxes into the immobile zone controlled
 279 by concentration gradients in the immobile zone alone.

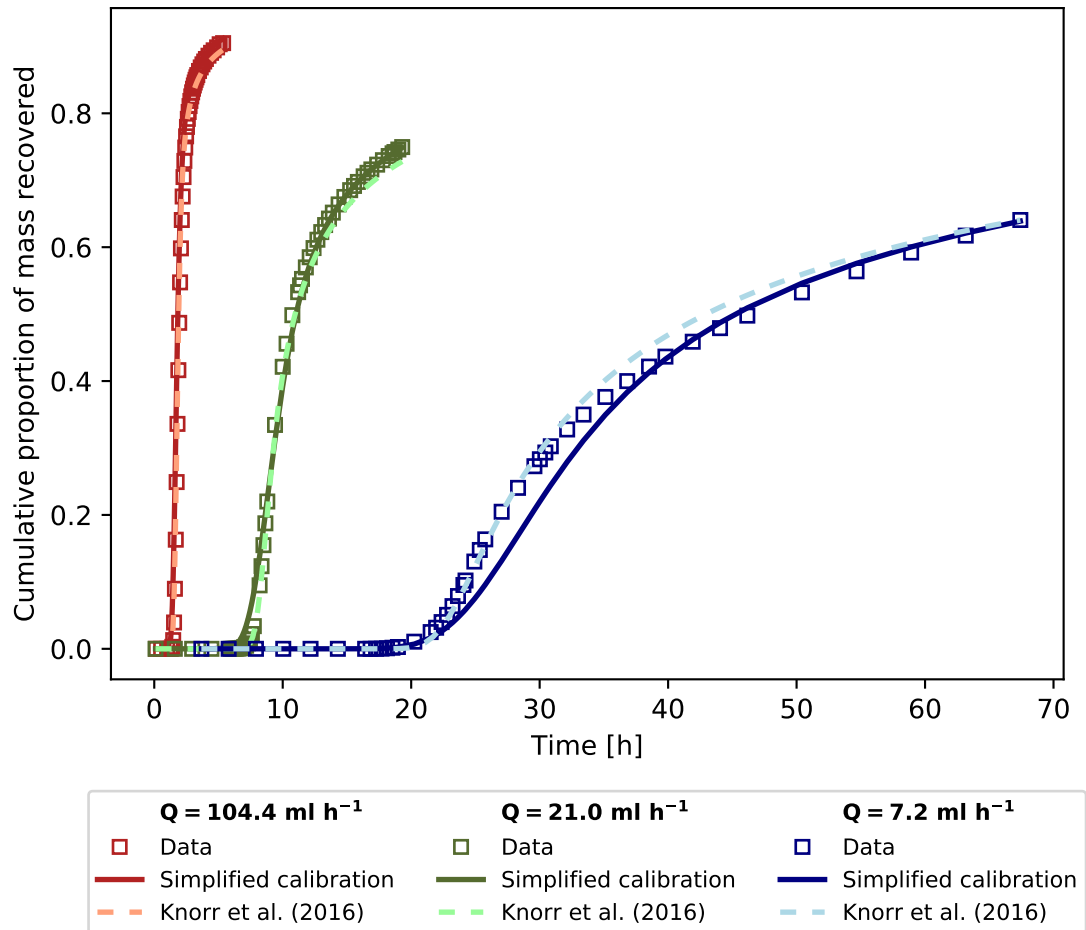


Figure 4. Simultaneous fit of three breakthrough curves collected in the column described by Knorr *et al.* (2016), at three different flow rates. Empirical breakthrough data (as adjusted per Appendix Appendix A) is indicated by empty squares, the original fits using (10) are indicated by dashed lines, and the joint calibration performed here is indicated by solid lines.

280 4 Summary discussion

281 4.1 The simplified approach is empirically supported

282 We re-analyzed two sets of bench-scale transport experiment data, one exhibiting
 283 HA and the other exhibiting MIMT, using the simplified approach to CTRW calibration
 284 that we previously derived. On this approach, the velocity-like and dispersion-like parameters
 285 in the CTRW GME are set equal to their Fickian counterparts, and the time constant
 286 is set to unity.

287 These results provide empirical support for the claims that mean groundwater velocity
 288 and a velocity-independent classical dispersivity suitable to domain scale can be employed
 289 directly in the CTRW GME, rather than the velocity-like and dispersion-like parameters
 290 v_ψ and D_ψ . It also supports the notion that $\psi(t)$ can be considered as a *temporal mapping*
 291 (subordination mapping) encoding the transition time alteration by physical processes
 292 not captured by mean advection (\bar{v}) and Fickian dispersion (D), namely MIMT and small-
 293 scale advective heterogeneity. The results simultaneously support the qualitative arguments
 294 underpinning the CTRW-on-a-streamline numerical approach which support the usage
 295 of a velocity-invariant $\psi(t)$ for HA and MIMT.

296 4.2 CTRW parameters cannot generally be interpreted in isolation

297 When interpreting the heterogeneous tank experiment, we parameterized a CTRW
 298 model with a TPL $\psi(t)$ featuring parameters much different from the previous calibration
 299 of Berkowitz and Scher. Most notably, both calibrations featured shared values of β and
 300 t_2 for all flow rates, but the calibrated values differ greatly between the two works. Li
 301 and Ren (2009) write "[t]he function $\psi(t)$ is the "heart" of the CTRW formation, dominating
 302 the principal characteristics of solute plume migration patterns...[t]he key factor is the
 303 interplay between β and the cutoff time t_2 , which has a dramatic effect on the entire shape
 304 of a migrating solute plume." The key point is the *interplay* of parameters in the model.
 305 Stronger statements implying that individual parameters may be interpreted in isolation
 306 are also found in the literature. For example, Shahmohammadi-Kalalagh and Beyrami
 307 (2015) write "the single parameter β quantifies all of the mechanisms that control the
 308 transport behavior". In this spirit, some authors only report the value of β when performing
 309 CTRW fits using TPL-distributed $\psi(t)$, but not t_1 or t_2 . (e.g., Xiong *et al.*, 2006; Shahmohammadi-
 310 Kalalagh and Beyrami, 2015; Frank *et al.*, 2020; Hu *et al.*, 2020), or report all TPL parameters

311 alongside v_ψ and D_ψ but do not report τ (e.g. Mettier *et al.*, 2006; Heidari and Li, 2014;
 312 Jiménez-Hornero *et al.*, 2005).

313 Our HA calibration above showed that the same set of experimentally-derived breakthrough
 314 curves can be parameterized with very different shared β and $t_2 - t_1$, both generating
 315 excellent, essentially indistinguishable breakthrough curve fits. This provides a cautionary
 316 counterexample to relating single CTRW parameters to underlying physics in isolation:
 317 one should report the complete transport description. This observation naturally extends
 318 to any mathematical formulation of $\psi(t)$, and to other superficially different approaches
 319 (e.g., multi-rate mass-transfer and fractional derivative models, see Berkowitz *et al.* (2006))
 320 that are special cases of the CTRW.

321 The need for this *particular* parameter set is tied to the use of (4): where one is
 322 working with explicit advective transitions, sometimes termed a time-domain random
 323 walk (Cvetkovic *et al.*, 2014; Hansen and Berkowitz, 2014; Cvetkovic *et al.*, 2016; Hansen
 324 and Berkowitz, 2020b), implicit advective transitions across voxels (Bijeljic *et al.*, 2011;
 325 Ederly *et al.*, 2014), or where calibration uses a first-passage distribution based on a pure
 326 power law $\psi(t)$ (Margolin and Berkowitz, 2000; Kosakowski *et al.*, 2001; Bromly and Hinz,
 327 2004), fewer parameters may be needed for a complete model description. In all cases,
 328 however, a complete model description must be reported to ensure meaningful, repeatable
 329 results, regardless of the model formulation.

330 As CTRW has demonstrated predictive validity (Fiori *et al.*, 2015), it is natural
 331 to relate its parameters to underlying physics by regression and other approaches. Recent
 332 examples include Ederly (2021), which explored the relationship between the difference
 333 $t_2 - t_1$ and conductivity field heterogeneity, and Frank *et al.* (2020) developed a regression
 334 relationship between β for a fracture transport and the Hurst exponent representing fracture
 335 roughness. In such efforts, we stress the need for a complete transport heterogeneity description
 336 when seeking physical interpretations; individual parameter values are not always uniquely
 337 constrained by physics. Fortunately, this additional complexity may be reduced without
 338 loss of generality on the simplified approach, as $(\alpha, \psi(t))$ represents a complete transport
 339 heterogeneity description, it is not necessary to include (v_ψ, D_ψ, τ) in an explanatory model.

Acknowledgments

We thank Prof. Brian Berkowitz for providing the original data for the HA flow cell experiment, Prof. Christine Stumpp for providing the original data for the MIMT column experiment, and both for helpful comments. All data used may also be digitized from the text and figures of Berkowitz and Scher (2009) and Knorr *et al.* (2016); no original data sets were employed in this paper. The work was supported by the Israel Science Foundation personal research grant 1872/19. SKH holds the Helen Unger Career Development Chair in Desert Hydrogeology at Ben-Gurion University.

References

- Abate, J.; P. P. Valkó, 2004. Multi-precision Laplace transform inversion. *International Journal for Numerical Methods in Engineering*, **60**(5), 979. 10.1002/nme.995.
- Berkowitz, B.; A. Cortis; M. Dentz; H. Scher, 2006. Modeling non-Fickian Transport in Geological Formations as a Continuous Time Random Walk. *Reviews of Geophysics*, **44**, RG2003. 10.1029/2005RG000178.
- Berkowitz, B.; H. Scher, 2009. Exploring the nature of non-Fickian transport in laboratory experiments. *Advances in Water Resources*, **32**(5), 750. 10.1016/j.advwatres.2008.05.004.
- Bijeljic, B.; P. Mostaghimi; M. J. Blunt, 2011. Signature of non-fickian solute transport in complex heterogeneous porous media. *Physical Review Letters*, **107**(20), 20. 10.1103/PhysRevLett.107.204502.
- Boano, F.; A. I. Packman; A. Cortis; R. Revelli; L. Ridolfi, 2007. A continuous time random walk approach to the stream transport of solutes. *Water Resources Research*, **43**(10), 1. 10.1029/2007WR006062.
- Bromly, M.; C. Hinz, 2004. Non-Fickian transport in homogeneous unsaturated repacked sand. *Water Resources Research*, **40**(7), 1. 10.1029/2003WR002579.
- Burnell, D. K.; S. K. Hansen; J. Xu, 2017. Transient modeling of non-Fickian transport and first-order reaction using continuous time random walk. *Advances in Water Resources*, **107**, 370. 10.1016/j.advwatres.2017.06.014.
- Cvetkovic, V.; A. Fiori; G. Dagan, 2014. Solute transport in aquifers of arbitrary variability: A time-domain random walk formulation. *Water Resources Research*,

- 371 **50**, 5759. 10.1111/j.1752-1688.1969.tb04897.x.
- 372 Cvetkovic, V.; A. Fiori; G. Dagan, 2016. Tracer travel and residence time
373 distributions in highly heterogeneous aquifers: Coupled effect of flow variability
374 and mass transfer. *Journal of Hydrology*, **543**, 101. 10.1016/j.jhydrol.2016.04.072.
- 375 Dentz, M.; A. Cortis; H. Scher; B. Berkowitz, 2004. Time behavior of solute
376 transport in heterogeneous media: Transition from anomalous to normal
377 transport. *Advances in Water Resources*, **27**, 155. 10.1016/j.advwatres.2003
378 .11.002.
- 379 Edery, Y., 2021. The effect of varying correlation lengths on anomalous transport.
380 *Transport in Porous Media*, **137**(2), 345. 10.1007/s11242-021-01563-9.
- 381 Edery, Y.; A. Guadagnini; H. Scher; B. Berkowitz, 2014. Origins of anomalous
382 transport in heterogeneous media: Structural and dynamic controls. *Water*
383 *Resources Research*, **50**, 1490. 10.1002/2013WR015111.
- 384 Fiori, A.; A. Zarlenga; H. Gotovac; I. Jankovic; E. Volpi; V. Cvetkovic; G. Dagan,
385 2015. Advective transport in heterogeneous aquifers: Are proxy models predictive?
386 *Water Resources Research*, **51**, 9127.
- 387 Frank, S.; T. Heinze; S. Wohnlich, 2020. Comparison of surface roughness and
388 transport processes of sawed, split and natural sandstone fractures. *Water*
389 *(Switzerland)*, **12**(9). 10.3390/w12092530.
- 390 Gaber, H. M.; W. P. Inskeep; S. D. Comfort; J. M. Wraith, 1995. Nonequilibrium
391 Transport of Atrazine through Large Intact Soil Cores. *Soil Science Society of*
392 *America Journal*, **59**(1), 60. 10.2136/sssaj1995.03615995005900010009x.
- 393 Haggerty, R.; S. A. McKenna; L. C. Meigs, 2000. On the late-time behavior of tracer
394 test breakthrough curves. *Water Resources Research*, **36**(12), 3467. 10.1029/
395 2000WR900214.
- 396 Hansen, S. K., 2020. Simplified calibration of continuous-time random walk
397 solute transport models. *Advances in Water Resources*, **137**, 103521. 10.1016/
398 j.advwatres.2020.103521.
- 399 Hansen, S. K.; B. Berkowitz, 2014. Interpretation and nonuniqueness of CTRW
400 transition distributions: Insights from an alternative solute transport formulation.
401 *Advances in Water Resources*, **74**, 54. 10.1016/j.advwatres.2014.07.011.
- 402 Hansen, S. K.; B. Berkowitz, 2020a. Aurora: A non-Fickian (and Fickian)
403 particle tracking package for modeling groundwater contaminant transport

- 404 with MODFLOW. *Environmental Modelling and Software*, **134**, 104871.
405 10.1016/j.envsoft.2020.104871.
- 406 Hansen, S. K.; B. Berkowitz, 2020b. Modeling non-Fickian solute transport due to
407 mass transfer and physical heterogeneity on arbitrary groundwater velocity fields.
408 *Water Resources Research*, **56**, e2019WR026868. 10.1029/2019WR026868.
- 409 Hansen, S. K.; C. P. Haslauer; O. A. Cirpka; V. V. Vesselinov, 2018. Direct
410 Breakthrough Curve Prediction From Statistics of Heterogeneous Conductivity
411 Fields. *Water Resources Research*, **54**(1), 271. 10.1002/2017WR020450.
- 412 Heidari, P.; L. Li, 2014. Solute transport in low-heterogeneity sandboxes: The role of
413 correlation length and permeability variance. *Water Resources Research*, **50**, 8240.
414 10.1002/2013WR014654.
- 415 Hu, Y.; W. Xu; L. Zhan; Z. Ye; Y. Chen, 2020. Non-Fickian solute transport in
416 rough-walled fractures: The effect of contact area. *Water (Switzerland)*, **12**(7).
417 10.3390/w12072049.
- 418 Huang, K.; N. Toride; M. T. Van Genuchten, 1995. Experimental investigation of
419 solute transport in large, homogeneous and heterogeneous, saturated soil columns.
420 *Transport in Porous Media*, **18**(3), 283. 10.1007/BF00616936.
- 421 Jiménez-Hornero, F. J.; J. V. Giráldez; A. Laguna; Y. Pachepsky, 2005. Continuous
422 time random walks for analyzing the transport of a passive tracer in a single
423 fissure. *Water Resources Research*, **41**(4), 1. 10.1029/2004WR003852.
- 424 Johansson, F.; *et al.*, 2021. *mpmath: a Python library for arbitrary-precision*
425 *floating-point arithmetic (version 1.2.0)*. <http://mpmath.org/>.
- 426 Knorr, B.; P. Maloszewski; F. Krämer; C. Stumpp, 2016. Diffusive mass exchange
427 of non-reactive substances in dual-porosity porous systems - column experiments
428 under saturated conditions. *Hydrological Processes*, **30**(6), 914. 10.1002/hyp.10620.
- 429 Kosakowski, G.; B. Berkowitz; H. Scher, 2001. Analysis of field observations of tracer
430 transport in a fractured till. *Journal of Contaminant Hydrology*, **47**(1), 29. 10
431 .1016/S0169-7722(00)00140-6.
- 432 Levy, M.; B. Berkowitz, 2003. Measurement and analysis of non-Fickian dispersion
433 in heterogeneous porous media. *Journal of Contaminant Hydrology*, **64**(3-4), 203.
434 10.1016/S0169-7722(02)00204-8.
- 435 Li, N.; L. Ren, 2009. Application of continuous time random walk theory to
436 nonequilibrium transport in soil. *Journal of Contaminant Hydrology*, **108**(3-4),

- 437 134. 10.1016/j.jconhyd.2009.07.002.
- 438 Maloszewski, P.; A. Zuber, 1990. Mathematical Modeling of Tracer Behavior in
439 Short-Term Experiments in Fissured Rocks. *Water Resources Research*, **26**(7),
440 1517.
- 441 Margolin, G.; B. Berkowitz, 2000. Application of continuous time random walks to
442 transport in porous media. *Journal of Physical Chemistry B*, **104**(16), 3942. 10
443 .1021/jp993721x.
- 444 Margolin, G.; M. Dentz; B. Berkowitz, 2003. Continuous time random walk
445 and multirate mass transfer modeling of sorption. *Chemical Physics*, **295**, 71.
446 10.1016/j.chemphys.2003.08.007.
- 447 Mettier, R.; G. Kosakowski; O. Kolditz, 2006. Influence of small-scale heterogeneities
448 on contaminant transport in fractured crystalline rock. *Ground Water*, **44**(5), 687.
449 10.1111/j.1745-6584.2006.00236.x.
- 450 Nelder, J. A.; R. Mead, 1965. A simplex method for function minimization. *The*
451 *Computer Journal*, **7**, 308.
- 452 Oliphant, T. E., 2007. Python for Scientific Computing. *Computing in Science and*
453 *Engineering*, **9**, 10. 10.1109/MCSE.2007.58.
- 454 Roberts, G. E.; H. Kaufman, 1966. *Table of Laplace Transforms*. W. B. Saunders
455 Company, Philadelphia.
- 456 Shahmohammadi-Kalalagh, S.; H. Beyrami, 2015. Modeling Bromide Transport in
457 Undisturbed Soil Columns with the Continuous Time Random Walk. *Geotechnical*
458 *and Geological Engineering*, **33**(6), 1511. 10.1007/s10706-015-9917-1.
- 459 Silliman, S. E.; E. S. Simpson, 1987. Laboratory evidence of the scale effect in
460 dispersion of solutes in porous media. *Water Resources Research*, **23**(8), 1667.
- 461 van Genuchten, M. T.; P. J. Wierenga; G. A. O'Connor, 1977. Mass Transfer
462 Studies in Sorbing Porous Media: III. Experimental Evaluation with 2,4,5-
463 T. *Soil Science Society of America Journal*, **41**(2), 278. 10.2136/sssaj1977
464 .03615995004100020023x.
- 465 Xiong, Y.; G. Huang; Q. Huang, 2006. Modeling solute transport in one-dimensional
466 homogeneous and heterogeneous soil columns with continuous time random walk.
467 *Journal of Contaminant Hydrology*, **86**(3-4), 163. 10.1016/j.jconhyd.2006.03.001.

Appendix A Correction of data in Knorr et al. (2016)

In Knorr *et al.* (2016), the authors present exit-time CDFs intended to correspond to (10), which have been numerically integrated from impulse response breakthrough curves that were measured. As reported, the impulse response curves should correspond to the function

$$\zeta(x, t) = \frac{a}{2\pi Q} \sqrt{\frac{x^2}{\alpha \bar{v}}} \int_0^s \exp \left[-\frac{(x - u\bar{v})}{4\alpha u \bar{v}} - \frac{a^2 u^2}{t - u} \right] \frac{1}{u(t - u)^3} du, \quad (\text{A1})$$

and $Q\zeta(L, t)$ should be the arrival time PDF at the exit of the column. As the integral of any probability distribution is 1, multiplying the reported impulse response data by Q and numerically integrating should yield 1, also. However, for the two lowest flow rates, this was not the case. Multiplying $Q\zeta(L, t)$ (as populated with the exact parameters reported by Knorr *et al.*) by the respective scaling factors 1, .82, and .625 for the flow rates 104.4, 21, and 7.2 ml h⁻¹, near-exactly reproduces the fitted impulse response curves shown in the paper. (See Figure A1 for illustration.) We verified that the CDFs reported were also generated by integration of the data shown (as pre-multiplied by Q), so the reported CDF data are off by the same factor and some total recovery rates were larger than previously shown.

Thus, the raw deuterium CDFs presented need to be multiplied respectively by 1, 1/.82, and 1/.625 to yield actual fraction recovered. We used these altered CDFs for the fitting work. We note that that the parameters in Knorr *et al.* actually also match the correctly re-scaled data when inserted into (10).

Appendix B Derivation of sojourn time PDF

We are interested in the time taken for a particle entering the immobile zone to complete its sojourn and exit. We map radial diffusion in the matrix onto a simple 1D lattice continuous-time random walk, and ask how long it takes for a particle introduced at node 0 at time 0 to return to node zero. We imagine that the lattice nodes are non-uniformly spaced (growing denser with greater radial distance), so that the transition statistics are the same for every node. Employing the observation of Knorr *et al.* that solute never reached the outside of the column, making the immobile domain an essentially infinite 1D diffusive sink, we work on a simple, infinite 1D lattice.

We define $R(x, t)$ as the ensemble average arrival rate of random walkers at node x time t , and $\psi(t)$ as the (location-independent) waiting time PDF for the time between

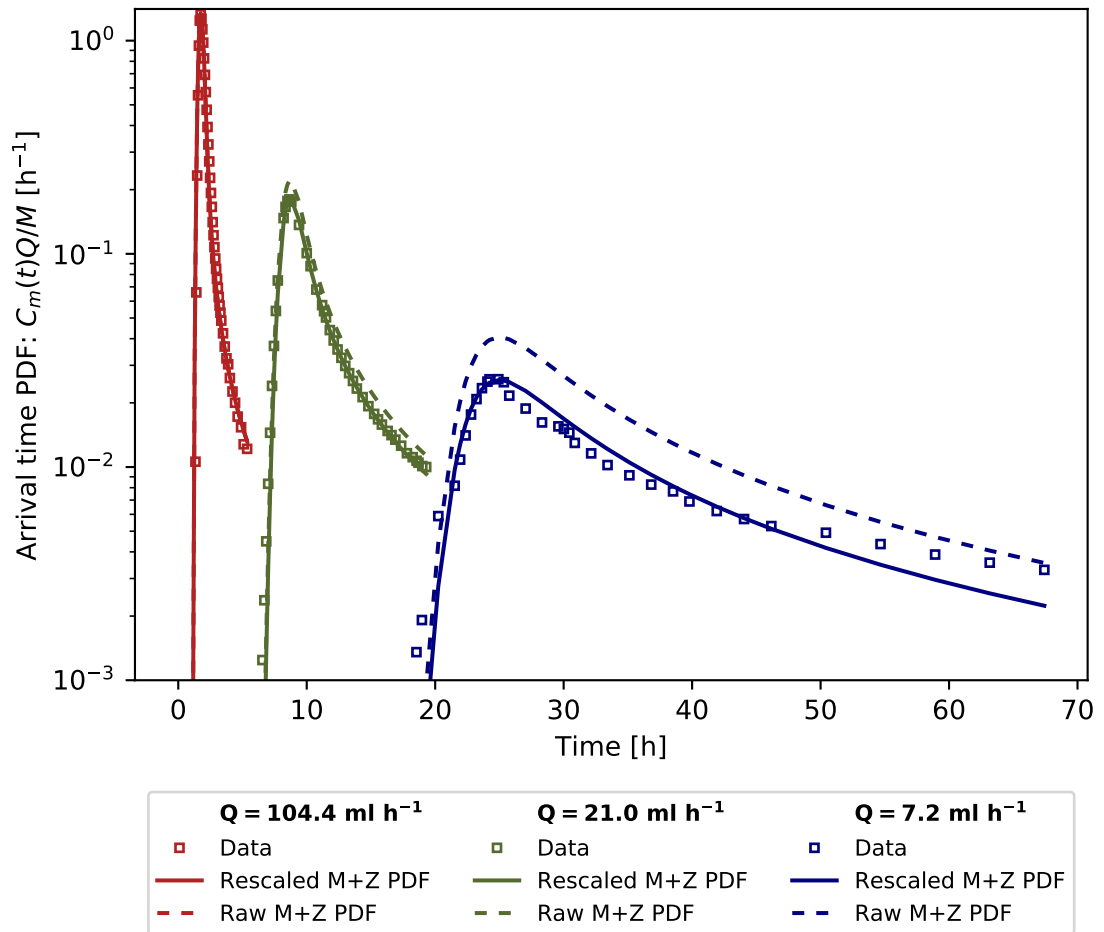


Figure A1. Data points presented in Knorr *et al.* (2016), along with raw evaluation of (A1) with parameters presented by Knorr *et al.*, and rescaled (A1) to best match the data points (and the curves shown by Knorr *et al.*).

498 two subsequent arrivals. Then, the ensemble average number of walkers, $P(x, t)$, at any
 499 given node, x , at time t may be expressed

$$P(x, t) = \int_0^t R(x, \tau) \Psi(t - \tau) d\tau, \quad (\text{B1})$$

500 where

$$\Psi(t) \equiv 1 - \int_0^t \psi(\tau) d\tau. \quad (\text{B2})$$

501 We consider a 1D system in which particles are introduced at $x = 0$ at $t = 0$ (this
 502 is the counterpart to immobilization under MIMT), and are interested in the *next* time
 503 the walker arrives at $x = 0$ (which we take to represent re-mobilization). We use the
 504 notation R_i to represent the arrival rate of only those particles that are arriving for the
 505 i -th time. Then we may write

$$R_1(0, t) = \delta(t), \quad (\text{B3})$$

506 and define the sojourn time PDF

$$\phi(t) \equiv R_2(0, t). \quad (\text{B4})$$

507 From recursive arguments, we may also conclude that:

$$R(x, t) = R_1(x, t) + \int_0^t R_2(x, \tau) R(0, t - \tau) d\tau, \quad (\text{B5})$$

508 and thus specifically that

$$R(0, t) = \delta(t) + \int_0^t \phi(\tau) R(0, t - \tau) d\tau. \quad (\text{B6})$$

509 Taking the Laplace transform and rearranging, yields

$$\tilde{R}(0, s) = \frac{1}{1 - \tilde{\phi}(s)}. \quad (\text{B7})$$

510 Transforming (B1) and applying it to the above equation yields

$$\tilde{\phi}(s) = 1 - \frac{\tilde{\Psi}(s)}{\tilde{P}(0, s)}. \quad (\text{B8})$$

511 In order to determine the transform for ϕ , we must determine the transforms on the RHS
 512 of (B8), which we may do from the well-known property that the variance σ_x^2 of a plume
 513 undergoing Fickian diffusion increases according to

$$\frac{d\sigma_x^2}{dt} = 2D, \quad (\text{B9})$$

514 where D here is not to be confused with D_ψ . Fickian diffusion from a point source at
 515 $x = 0$ is known to be described by a Gaussian distribution. At $x = 0$ the exponential
 516 portion of the distribution becomes unity and, mapping to a discrete-site approach with
 517 spacing Δ_x , it follows that

$$P(0, t) = \frac{\Delta_x}{\sqrt{4\pi Dt}} = \frac{1}{2\pi\mu t}, \quad (\text{B10})$$

518 where we define $\mu \equiv 2D/\Delta_x^2$. Taking the Laplace transform (Roberts and Kaufman,
 519 1966), it follows that

$$\tilde{P}(0, s) = \frac{1}{\sqrt{2\mu s}}. \quad (\text{B11})$$

520 We can similarly argue from (B9) that μdt is the constant probability of completing a
 521 diffusive transition to a neighboring site in a short increment of time dt , implying that
 522 $\psi(t) = \mu e^{-\mu t}$, and

$$\tilde{\Psi}(s) = \frac{1}{s + \mu}. \quad (\text{B12})$$

523 Inserting (B11) and (B12) into (B8) yields our final result (7), repeated here for clarity
 524 of presentation:

$$\tilde{\phi}(s) = 1 - \frac{\sqrt{2\mu s}}{s + \mu}.$$

526 By numerical inversion, we can see that the distribution defined by $\phi(t)$ is closely
 527 approximated by $\text{Pareto}(\mu^{-1}, \frac{1}{2})$, where the first argument is the scale parameter, and
 528 $\frac{1}{2}$ is the shape parameter (power law exponent). This agrees with the with Haggerty *et al.*
 529 (2000) who reported the return time for diffusion in an infinite slab as power-law distributed
 530 (with exponent $\beta = 0.5$). Examples are shown in Figure B1.

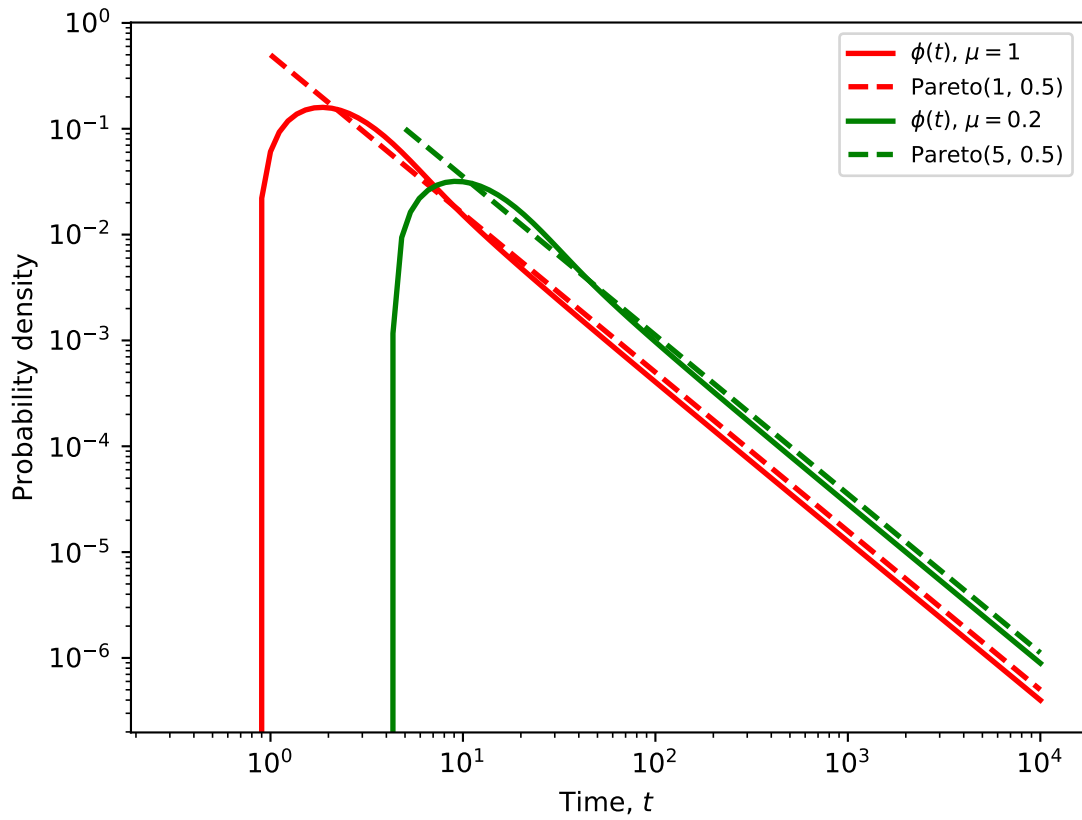


Figure B1. Graphs of $\phi(t)$ obtained from numerical inversion of (7) and corresponding Pareto approximations for two values of μ .